Chapter 8

Evolution of Drainage in Response to Brittle - Ductile Dynamics and Surface Processes in Kachchh Rift Basin, Western India

Girish Ch Kothyari, Ajay P. Singh, Sneha Mishra, Raj Sunil Kandregula, Indu Chaudhary and Gaurav Chauhan

Additional information is available at the end of the chapter

http://dx.doi.org/10.5772/intechopen.73653

Abstract

The eastern part of Kachchh Rift basin was reactivated after 2001 Bhuj earthquake of Mw 7.7 and continuous seismicity has been recorded since then. The northern part of Wagad upland also experienced moderate earthquakes Mw ≥ 5.7 in February 2006 and March 2007. These moderate to major Intraplate earthquakes provide a unique opportunity to study the effects and linkage between brittle-ductile dynamics, surface processes and drainage evolution. We presented a geomorphological analysis of the Wagad highland providing new constraints on the evolution of river network. The shallow to deeper nature of fault and their response to development of hydrological networks has been analyzed using seismic tomography. Based on surface drainage offset and seismic structures several E-W oriented faults controlling fluvial dynamics are identified. From seismic structures and drainage offset it is clear that the fluvial dynamics is controlled by shallower to deeper faults. The estimated attributes are well supported with seismic structures and focal mechanisms solutions. Based on fluvial offset and seismic structure analysis a new tectonic model has been proposed for WH. The tectonic model shows that the faults WH are well connected at deeper level and generated negative flower structures and significantly controlling surface fluvial dynamics.

Keywords: drainage, geomorphology, fluvial dynamics, seismic structure, focal mechanisms

1. Introduction

Spatial distributions of geomorphic landforms in active regions are the results of the complex interaction of shallow and deep earth processes [1]. The imprints of these processes are reflected in the form of changes of local relief, drainage pattern, hypsometry, steepness, and channel slope relationship [2–8]. These parameters can be used to quantitatively characterize the relationship between shallow and deeper crustal structure, and geomorphic processes [1, 9]. The dry land fluvial systems of intraplate Kachchh rift basin, allow us to study the effects and linkage between brittle - ductile dynamics and surface processes on landscape evolution. The Kachchh basin evolved during the Early Jurassic, bound by Nagar Parkar Fault to the north and North Kathiawar Fault to the south (**Figure 1A**). The rifting was aborted by the trailing edge uplift during the Late Cretaceous pre-collision stage of the Indian plate, when the leading edge of the plate was slab-pulled towards the Tethyan trench [10, 14, 16]. Lateral motion during the drift stage of the plate induced horizontal stress and near vertical normal faults, which were reactivated as reverse faults during initiation of the inversion cycle, and became strike-slip faults involving divergent oblique-slip movement [10, 14, 17, 18].

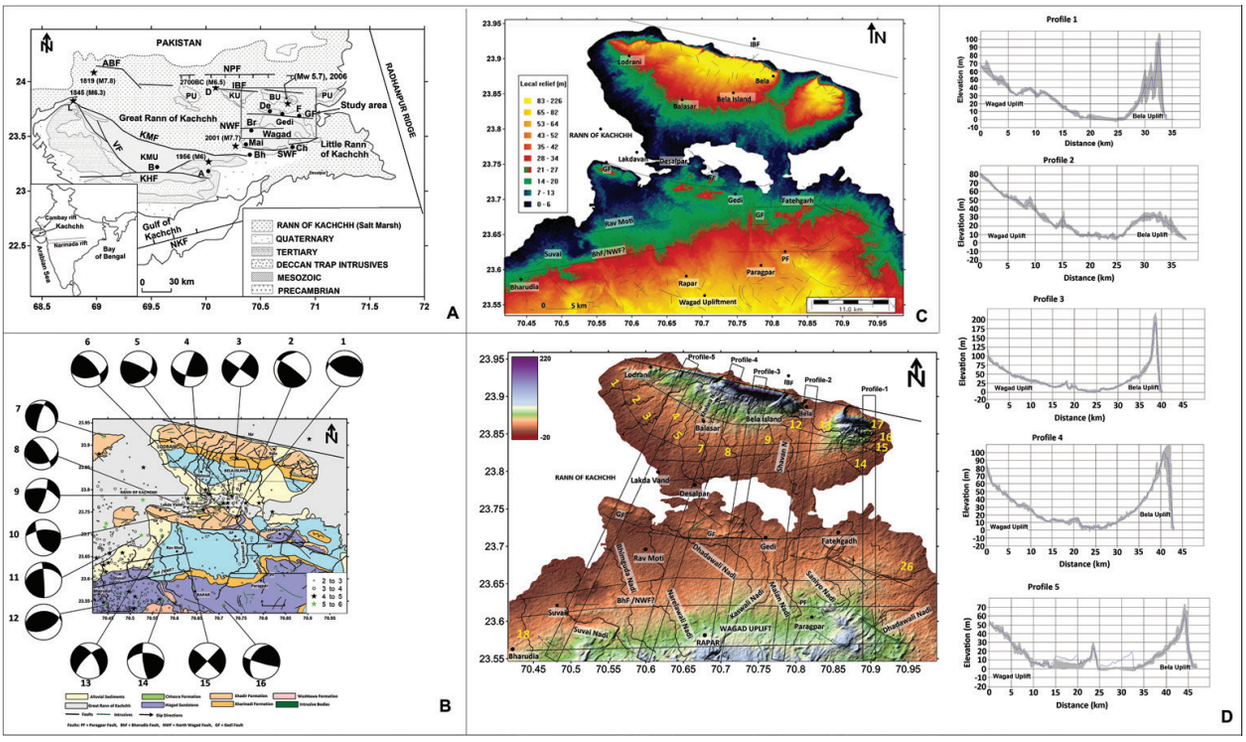

Figure 1. (A) Seismotectonic map of the Kachchh rift basin integrated with the geological map, showing the epicenters of significant earthquakes (modified after [10]). The Wagad area lies between the SWF and GF. Locations - A (Anjar), B (Bhuj), Ba (Bhachau), Br (Bharudia), Ch (Chitrod), D (Dholavira), De (Desalpar), L (Lakhpat), F (Fatehgarh) and G (Gedi); faults: NKF (North Kathiyawad Fault), KHF (Katrol Hill Fault), VF (Vigodi Fault), KMF (Kachchh Mainland Fault), SWF (South Wagad Fault), NWF (North Wagad Fault), GF (Gedi Fault), IBF (Island Belt Fault), ABF (Allah Bund Fault) and NPF (Nagar Parkar Fault); uplifts: KMU (Kachchh Mainland Uplift), PU (Patcham Uplift, KU (Khadir Uplift), BU (Bela Uplift), CU (Chorar Uplift). (B) Geological map of northern Wagad highland region [11]; shows location of earthquake epicenters. Focal mechanisms (1–16) plotted in the figure are after [12–15]. (C) CARTOSAT-DEM driven local relief map of Wagad Highland. Major and minor faults are marked by solid black line. (D) CARTOSAT DEM of the study and location of the five swath profiles; 1–5) swath profiles show the trends of the maximum, minimum and mean topography of the Wagad region. **Figure 1A** and **1B** *have been digitized in Surfer 14 software, while, we used MICRO-DEM 10 software for generation of* C and D, *and final editing has been done in golden software Surfer 14.*

http://dx.doi.org/10.5772/intechopen.73653

Major structural features of the Kachchh region include east – west trending active faults [16, 19] (**Figure 1A**). The Wagad highland (WH) of Kachchh is bounded by the South Wagad Fault (SWF) in the south and Gedi Fault (GF) in the north comprises of Mesozoic sediments overlying a granitic basement [16]. The initiation and steadiness of dynamics support beneath Kachchh basin have been explored in several studies [10]. Earlier researchers argued that the impingement of a large intrusive body in the lower crust [19–21]. However, the fault adjacent to intrusive body at deeper depth gradually flattens close to magmatic body owing to listric nature of fault [20, 22]. The fault model proposed by [10] suggests that the GF is a sub-vertical fault and gradually changing listric nature in lower crust.

The chronometric and geomorphic attributes of the GF, suggests that the region is uplifting at the rate of 0.3–1.1 mm/y during the last 9 ka [23]. The results of geomorphic processes and subsurface dynamics of GF zone can be explored by investigating how base level fall at the WH region propagates through the drainage network. The subsurface nature of faults in WH and their association with landscape evolution is still unknown. However, in present study an attempt has been made to understand brittle and ductile dynamics of fault system controlling surface landscape pattern. In this study first time we proposed an integrated sub surface model of WH by combining seismic structure (Tomograph) and surface geomorphology. In this connection we analyzed the 27 basins of WH. In particular**,** we investigated the general topographic features e.g. swath profiles, local relief and the river network (river longitudinal profiles). We employed a knickpoint celerity approach in order to provide a chronological framework to the evolution of the river network. Furthermore, we made an attempt to image subsurface fault pattern of the area using the seismological approaches such as tomoDD and focal mechanisms. The results permitted us to trace the long-term evolution of the WH, to confirm dynamic support and documenting its impact on the contrasting development of the drainage basins.

2. General geomorphology and seismicity of Wagad Kachchh

The WH is second largest uplifted block of Kachchh basin, after mainland of Kachchh, covering an area of ~2432 km^2, and is bounded by GF to the north and SWF to the south [11, 16]. The area is drained by numerous ephemeral streams; flow direction regularly spaced around the upper planation surface [23, 24]. From north to south, the WH comprises of three E-W trending active faults, namely the GF between Deshalpar and Fatehgarh area, the North Wagad Fault (NWF) north of Bharudia and the SWF between Mai and east of Chitrod (**Figure 1A**).

Geomorphologically the WH is divided into 3 units; (i) the upper planation surface (Mesozoic) with juvenile streams, (ii) the middle incised slopes with piedmont (Tertiary), and (iii) the low-lying areas representing Quaternary deposits [23, 25]. The upper surface represents an early Quaternary erosional event, whereas the middle incised slopes with terraces were developed during late Quaternary [26]. These two geomorphic units provide sediments to the lower peripheral areas. Suvai, Bhimguda, Narelawali, Dhadawali, Karaswali, Malan, Baniyo, and Dabhodanwari are six ephemeral rivers that flow northward and originate from the WH, following the regional slope and drain into the Great Rann of Kachchh [23]. Along their longitudinal length, these rivers cross several E-W oriented faults (**Figure 2**).

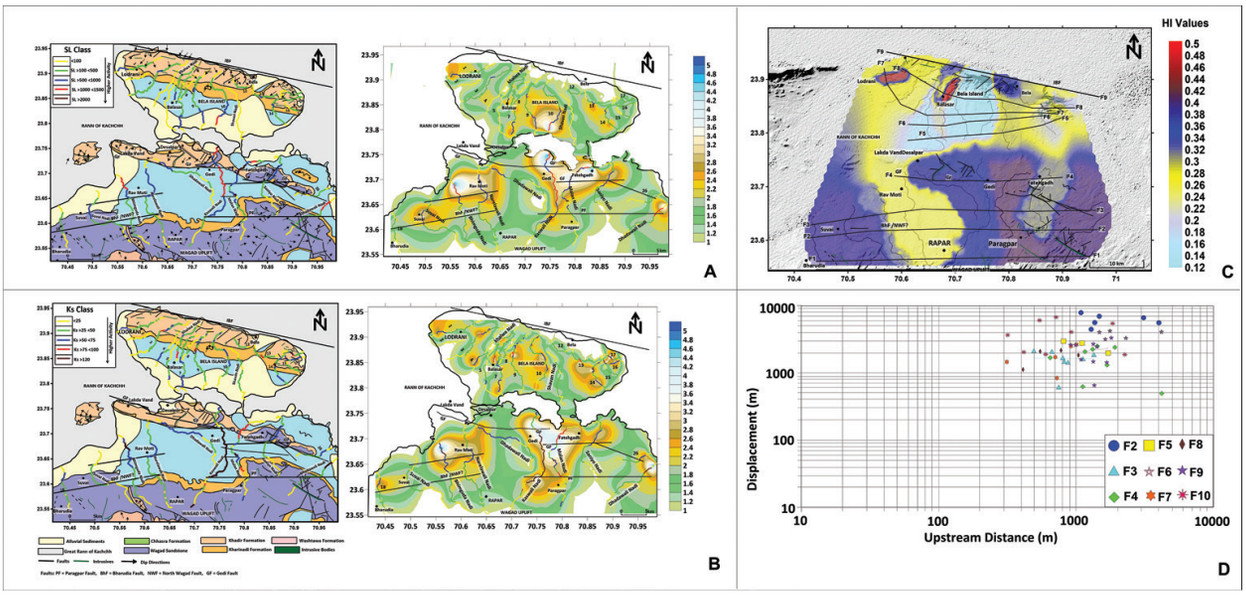

Figure 2. (A) Geological map of Wagad area shows especial distribution of SL along various geological units. Spatial distribution of SL class contour map of northern Wagad region. The higher activity is marked by higher order color (B) especial distribution of Ks along various geological units. Distribution of Ks class contour of northern Wagad region. Fault lines are shows by solid black line; dykes are marked by green lines; and bedding slope direction is highlighted by small black arrow. (C) Spatial variation of topography and statistics estimation for values of basin-wide hypsometric integral. The hotspots of higher uplift are marked by higher color values of hypsometric integral. (D) Relationship between amounts of stream offset along the fault and upstream length from the faults (F1–F10). *For generation of* **Figure 1A** and **B** *used Arc-GIS-10.4, Global mapper 18 software's and the final editing and contouring has been done in Surfer-11 software. We used River tool 3.0 for generation of hypsometric curves. The contour values of hypsometry Integral (HI) has been generated in Global mapper 18 and finally the contouring has been done in Surfer 14 software. We used excel for generation of* **D**.

The aftershocks of the January 26, 2001 Bhuj earthquake (Mw 7.7) are still continuing [15]. Distribution of the hypocenter of these aftershocks suggests that they are distributed mainly towards NE and SW directions. It has been observed that the WH is pronounced activated after the 2001 mainshock [12, 15, 27]. It is testified by a large number of aftershocks (Mw ≥ 2.5) occurred in the WH with focal depths ≥10 km. A few moderate earthquakes also occurred along the GF. Among these earthquakes, the most recent are the February 2006 (Mw 5.0); February 2006 (Mw 4.8); March 2006 Mw 5.7 and April 2008 Mw 4.1 [27] (**Figure 1B**). In the GF zone some 30 earthquakes (Mw 3.0–5.7) have been recorded at Seismic Network of Gujarat (SesisNetG) at shallow focal depths (≤ 20 km) during the period of 2006–2013 (**Figure 1B**).

3. Data and methodology

To investigate the relationship between brittle - ductile dynamics and surface processes in northern Wagad, we focused on topographic features (filtered topography, swath profiles, local relief), and hydrography (river longitudinal profiles), We used two elevation data sources: the CARTOSAT 2.5 m resolution digital elevation data (http://bhuvan.nrsc.gov.in) for regional scale analysis and the SRTM (http://srtm.csi.cgiar.org) of 90 m resolution for detailed analysis. Seismic tomography has been used to evaluate shallower to deeper surface dynamic

http://dx.doi.org/10.5772/intechopen.73653

process. The digital elevation model extracted from the SRTM was validated with the Survey of India topographic map (1:50,000) scale. To extract drainage network DEM data is used and 27 northward and south ward flowing rivers basins were generated. We calculated several tectonic attributes namely stream length-gradient Index (SL); steepness index (Ks), hypsometric integral (HI), asymmetric factor (AF) and Basin shape (BS). Based on results obtained from above analysis, spatial distributions of relative index of active tectonics (RIAT) are estimated for North Wagad/Bharudia, Gedi and Island fault zones. The dimensions of these drainage basins are given in **Table 1**.

3.1. Map of local relief

The map of local relief in the present study is produced from River-Tool by subtracting arithmetically a sub-envelope surface that describes the general pattern of valley bottoms elevations from an envelope surface (that connects peaks elevations) [28]. We obtained such surfaces by smoothing the minimum and maximum topography of the SRTM DEM by a 20 km wide circular moving window (**Figure 1C**). We chose the value of 20 km since it is the average spacing of the main valleys (5th, 6th and 7th Strahler order with respect to a critical area of ~4 km^2). This allowed us to remove small valleys, in effect operating like a low-pass filter that highlights the regional-scale features.

3.2. Swath profiles

We have considered five swath profiles across the study area to describe and quantify the topographic trend of the northern WH. The results show the trend of minimum, maximum and mean elevation into a single plot [29, 30] (**Figure 1D**). The statistical analyses such as maximum, minimum and mean elevations were calculated along each swath profile within a GIS platform. (**Figure 1D**). A rectangular swath of 300 m width was chosen to extract a series of parallel profiles that are separated by 1-cell (5 m). The width of the swath profile has been used to condense both elevated surfaces and streams. The higher elevation in swath depicts maximum elevation corresponds to the ridgelines; whereas, the lower elevation curve for the minimum elevation represents the valley floors. The Incision by river can be measured by the arithmetic difference between the maximum and minimum elevations within the longitudinal distance of the swath rectangle [31].

3.3. Stream length gradient index (SL)

The SL index is one of the quantitative geomorphic parameters included in morphotectonic assessment (Hack, [34]). This index will increase in value as rivers and streams flow over active uplifts and may have lesser values when flowing parallel to structures such as valleys made by strike-slip faulting [32]. The SL index seems to be a valid tool to detect local uplift as well as the incipient local response to regional processes [33]. Conventionally the SL index shows a quantitative approach to differential geomorphic studies related to erosion and depositional processes that include the river channel, long profile, and valley morphology as well as tectonically derived features such as fault scarps. This index was defined by [32] as:

Basins	Area (km²)	Area %	AF	BS	SL class	Ks class	HI class	AF class	BS class	RIAT value	RIAT class
1	30.759	2.05	7.70	3.4	2	2	2	2	4	2.4	3
2	8.962	0.60	1.90	3.2	1	1	4	1	4	2.2	2
3	49.538	3.31	14.21	3.4	2	2	2	2	4	2.4	3
4	22.855	1.53	16.59	5.3	1	2	2	3	5	2.6	3
5	49.991	3.34	12.06	4.8	1	2.5	1	2	5	2.3	3
6	17.051	1.14	5.12	3.9	2	2	3	2	4	2.6	3
7	20.658	1.38	15.41	5.4	2	2	2	3	5	2.8	4
8	7.733	0.52	13.51	3.6	1	1	4	1	4	2.2	3
9	56.53	3.77	3.60	3.5	2	2	1	1	4	2	3
10	52.989	3.54	8.07	2.8	2	2	1	2	3	2	3
11	40.325	2.69	1.48	3.6	1	1	2	1	4	1.8	1
12	20.395	1.36	8.76	1.5	1	2	3	2	2	2	2
13	11.269	0.75	5.24	3.2	2	2	3	2	4	2.6	3
14	13.33	0.89	14.92	6.2	2	2.5	2	2	5	2.7	4
15	16.705	1.12	35.33	1.6	1	1	2	4	2	2	2
16	9.342	0.62	20.88	3.4	1	2	1	3	4	2.2	3
17	5.188	0.35	4.82	3.7	1	3	2	1	4	2.2	3
18	53.91	3.60	25.82	2.3	1	2	3	4	3	2.6	3
19	134.73	8.99	10.92	1.6	2	1	3	1	2	1.8	1
20	48.422	3.23	13.31	9.4	2	2.5	3	1	5	2.7	6
21	209.47	13.98	8.26	1.9	2	2	2	2	2	2	2
22	71.57	4.78	15.51	3.7	2	2	3	1	4	2.4	3
23	151.26	10.10	3.18	3.9	3	3	3	1	4	2.8	5
24	129.46	8.64	14.02	4.9	3	2.4	4	2	5	3.28	5
25	96.119	6.42	4.32	2.5	2	2	3	1	3	2.2	2
26	64.618	4.31	31.38	1.9	1	2	4	1	2	2	2
27	104.85	7.00	2.10	1.5	2	2	4	1	2	2.2	3

Table 1. Spatial distribution of SL, HI, AF, Smf, SI, Bs, RSS, RIAT classes.

$$SL = (\Delta H/\Delta L)^{*} L \tag{1}$$

where $\Delta H/\Delta L$ is the local slope of the channel segment being evaluated, and L is the channel length from the divide to the midpoint of the channel reach. The SL index value increases as

streams flow over active uplifts and areas with high rock resistance and may decrease with low rock resistance. The integrated plot of stream longitudinal profile and SL index of all the rivers are presented graphically on the x- and y-axis of the longitudinal profile of the main channel (**Figure 3**).

3.4. Steepness index (Ks)

The normalized channel steepness index could be expected to vary with rock uplift rate (relative to base level), lithology, and climate [34, 35]. The method used for evolution of steepness index in the study area is based on the empirical power law equation of [36, 37] that relates the local slope (S) to the upstream contributing drainage basin area (A) [37, 38], However in present paper similar methodology has been:

$$S = k_s A^{-\Theta} \tag{2}$$

where k_s is the steepness index and Θ is concavity. Given Flint's law, the relationship between drainage area and distance downstream often described with Hack's law strongly influences the rate of change in channel gradient with distance downstream, which of course defines the concavity of river profiles. If there is no differential uplift, the value of Ks should remain constant. In the case of the river basin is undergoing differential uplift, Ks may change from one segment to another [38].

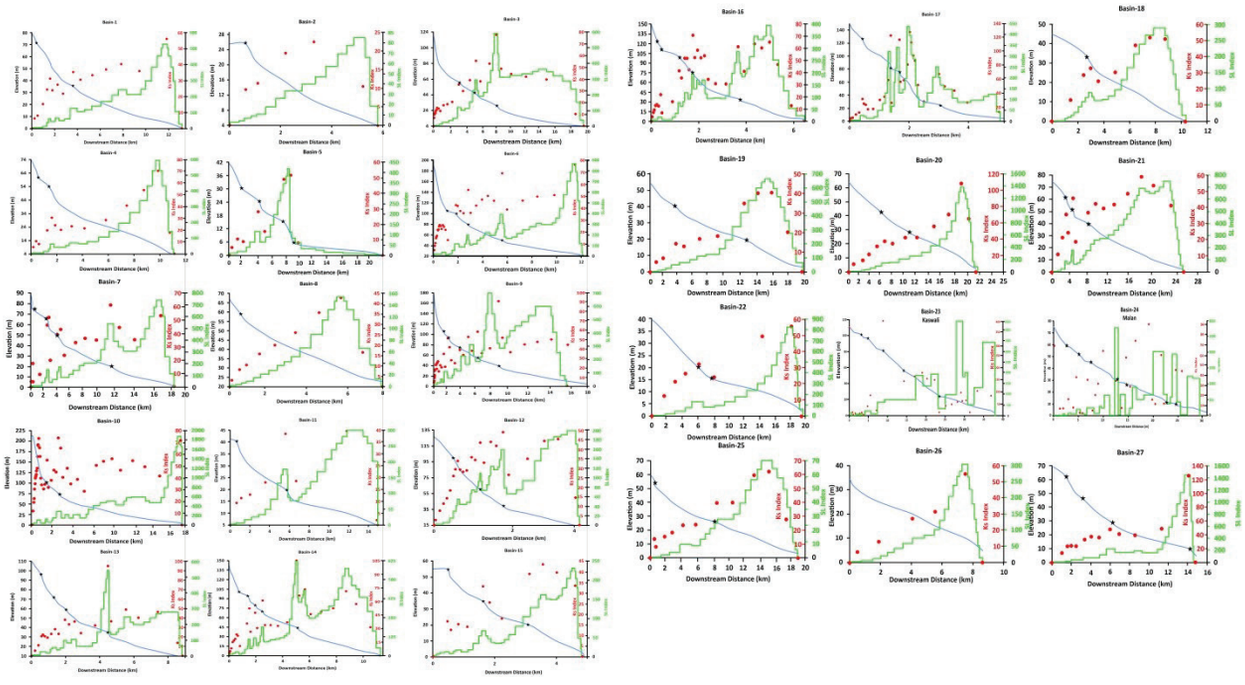

Figure 3. Integrated longitudinal river profiles and SL index of eight representative, rivers (Note: For details of all integrated river profiles, see **Figure 3**, SL is shown by small green line along the profile; solid thick red dots represents values of Ks along the long profile; knickpoints are marked by black star. *After collecting data in Arc GIS we used Microsoft excel for generating long river profiles and final editing has been done in golden software Surfer 14.*

3.5. Hypsometric integral (HI)

The hypsometric integral is an index that describes the distribution of elevation of a given area of a landscape [39]. The integral is generally derived for a particular drainage basin and is an index that is independent of basin area. The index is defined as the area below the hypsometric curve and thus expresses the volume of a basin that has not been eroded. The simple equation that may be used to calculate the index [32, 40] is:

$$HI = (average\ elevation - minimum\ elevation)/(maximum\ elevation - minimum\ elevation) \quad (3)$$

The hypsometric curve indicates degree of dissection of the basin, i.e., erosional stage of the basin. Concave profiles represent long-term equilibrium between uplift and erosion rates. Concave – convex profiles with erosion steps in the middle reaches indicate long-term predominance of erosional processes. Convex profiles are characteristic of areas where uplift (active tectonics) is dominant [41] The area below the hypsometric curve is known as the hypsometric integral (HI). The value of HI varies from 0 to 1 [41–43]. These profiles are drawn by projecting rivers onto a theoretical pre-incision surface that is obtained by interpolating the altitudes from present-day lateral divides of the basins (**Figure 4**). The values of elevation necessary for the calculation are obtained from a digital elevation mode.

3.6. Basin asymmetry (AF)

The asymmetric factor (AF) is a way to evaluate the existence of tectonic tilting at the scale of a drainage basin. The method may be applied over a relatively large area [32, 41] AF is defined by:

$$AF = 100\ (Ar/At) \quad (4)$$

where Ar is the area of the basin to the right (facing downstream) of the trunk stream and At is the total area of the drainage basin. If a basin has developed under stable conditions with little or no tilting, the Af factor is close to 50. The index is sensitive to change in inclination perpendicular to the channel direction. An AF factor above or below 50 may result from basin tilting, resulting either from active tectonics or lithologic, structural control, differential erosion. The AF value ranges from 18 to 85. The absolute difference (AF-50) has been calculated and the obtained values are grouped into four classes: class-1 ($AF \leq 5$; symmetric basins), class-2 ($6 \leq AF \leq 15$; gently asymmetric basins), class-3 ($16 \leq AF \leq 25$; moderately asymmetric basins), and class-4 ($AF \geq 26$; strongly asymmetric basins) (**Table 1**). The area of these drainage basins corresponding to asymmetric values is shown on the map (**Figure 5A**).

3.7. Basin shape (Bs)

The horizontal projection of a basin may be described by the basin shape index or the elongation ratio, Bs [43]:

$$Bs = Bl = Bw \quad (5)$$

http://dx.doi.org/10.5772/intechopen.73653

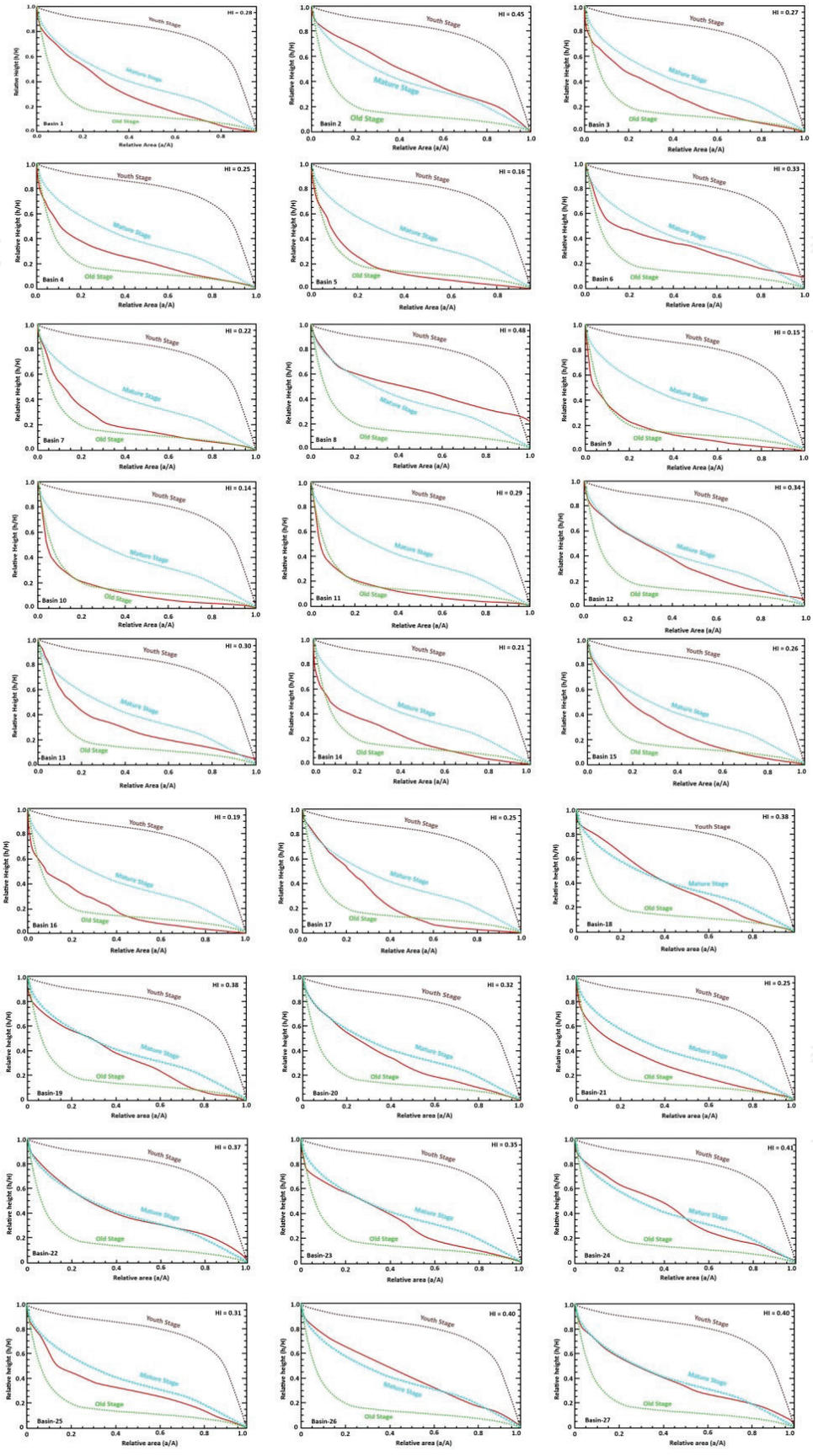

Figure 4. Hypsometry curves of all river basins integrated with youth (brown color), mature (cyan color), and old stages (green color) of river basin. *The hypsometric curves has been generated using River Tool 3.0 software and final editing has been done in golden software Surfer 14.*

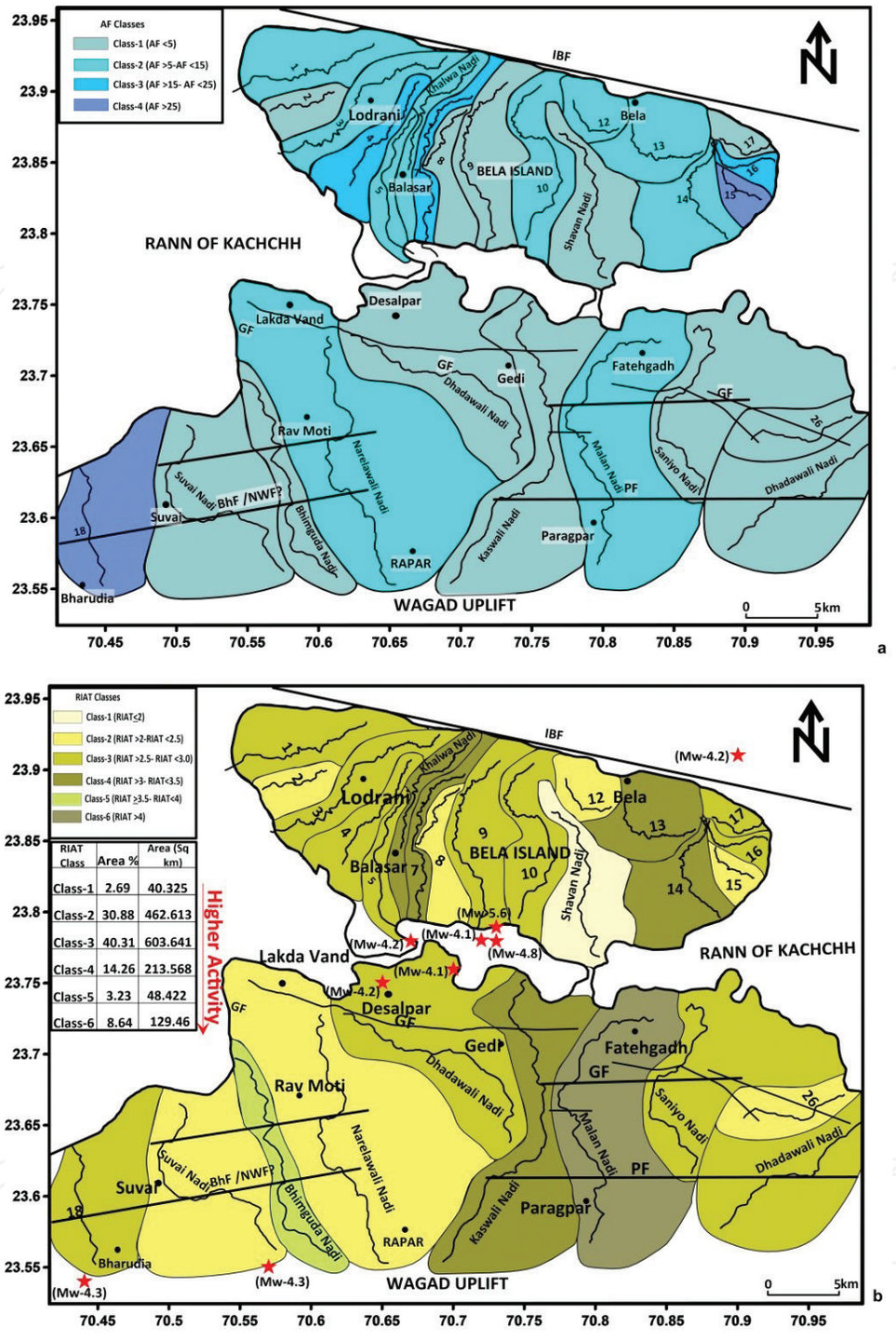

Figure 5. A spatial distribution of basin asymmetry along the northern Wagad area. (B) Estimated relative index of active tectonics (RIAT) distribution pattern of the area. A *and* B *have been generated using Global mapper 18 software and the final editing has been done in surfer 14 software.*

where *Bl* is the length of a basin measured from the highest point, and *Bw* is the width of a basin measured at its widest point. Relatively young drainage basins in tectonically active areas tend to be elongated in shape, normal to the topographic slope of a mountain [41, 43]. Therefore, *Bs* may reflect the rate of active tectonics.

http://dx.doi.org/10.5772/intechopen.73653

4. Relationship between fault displacements and drainage offset

Conventionally, quantitative displacement in a fault zone has been demonstrated by an offset of the river channel [25, 44, 45]. Usually, it has been widely observed that the maximum displacement occurred in the central part of the fault zone [46] and that the displacement decreases with increasing length. Decrease of river offset towards the west is possibly, westward propagation of the faults. These streams were taken into account to calculate offset ratio:

$$a = D/L \tag{6}$$

where D is the amount of stream offset along fault and L is upstream length of the displaced stream [47]. A relationship between long-term slip rate (S) along the lateral slip of a fault and offset ratio ($a = D/L$) has been roughly calculated as S (m/1000 years), *i.e.,* 10 a [25, 44, 45].

We investigated the major to north flowing rivers such as the Suvai, Bhimguda, Narelawali, Dhadawali, Karaswali, Malan, Baniyo, and Dabhodanwari rivers and adjoining streams to estimate river offset along the E-W faults F1–F4 (GF). However, 17 south flowing rivers such as 1–8, Khalwa River (9), 10, 11, Sharan Nadi (12), and rivers 13–17 have been analyzed to estimate offset along faults F6–F8. Based on offset of river channel we estimated net displacement along F2–F10 respectively.

5. Relative index of active tectonics (RIAT)

Several remote sensing studies have used the geomorphic indices to obtain index of relative tectonic activity [48–50]. To understand the RIAT of the fault segments, the results of all calculated geomorphic indices were synthesized. In this study we used geomorphic indices of active tectonics to obtained RIAT for the (NWF) North Wagad Fault, (GF) Gedi Fault, Bharudia Fault and (IBF) Island Belt Fault. Based on these classes we have considered each basin class average and combined to obtain the RIAT. The values of RIAT is assigned into five classes as Class- VI (RIAT >4), Class V: (> 3.5 RIAT <4), Class IV: (>3 RIAT <3.5), Class III: (>2.5 RIAT <3), Class II (>2 RIAT <2.5), and Class I (RIAT <2), (Supplementary Table 1; **Figure 5B**). Depending on the relative index of active tectonics classes, Western part of Wagad uplift covering basin 11, and Easterly covering 15 and 16 comes in highly active zone and shows offsetting drainage pattern (Class 5). Basin 1, 3, 4, 7 and 10 in Bela island, basin 13 and 18 in Wagad uplift are tectonically active and comes in (Class 4) zone and also delimiting by transverse fault between Basin 5, 6 and 9 in Bela Island 12, 14 and 17 in Wagad uplift are moderately active zones (Class 3) (**Figure 5B**). Basin 2 is intermediately active and comes in (Class 4) and Basin 8 is low active region.

6. Seismological approaches

The evidences of geomorphological in the Kachchh Rift Basin (KRB) is also supported by available high resolution seismic structures, fault plane solutions and recorded seismicity at

SeisNetG [13, 15, 51]. Theses integrated approaches provide a clue to understand what instigate to generating a negative flower structure of drainage patterns and its role in the seismicity in the regions. The snapshot of the seismic images play important role to understand brittle-ductile dynamics. It also shed light about hidden causative faults and the drainage patterns that can dictate the degree of damage through shaking (**Figure 1B**). Several faults in the Kachchh areas are mapped on the surface but still there are many among the existing factory of faults which still remains undiagnosed and not mapped on the surface [15, 51]. That is why we have determined almost all geological evidences and crustal heterogeneities parameters in the present study to understand the nature and extent of underlain structures controlling drainage network. The available 16 fault-plane solutions of the inferred fault planes of the events (Mw ≥ 3.5) recorded during 2007–2014 [13, 15, 51] (**Figure 1B**). The results obtained from morphotectonic analysis of fluvial networks and seismological approaches are jointly analyzed in the next section.

7. Imprints of active tectonics

The rivers in WH containing the knickpoints over the Mesozoic formations; are related to active geological structures. The maps of local relief, swath, stream length gradient index, and channel steepness (**Figures 1D** and **2**) represents two major topographic zones. The high elevated zones are located between 28 and 228 m. The high relief locations represent remnants of a relict landscape that was preserved at high elevations caused by erosionally balanced rapid Late Quaternary uplift [23]. The low relief zones are marked by Banni and Rann surfaces (**Figure 1C**). The DEM generated swath profiles shows incision into the alluvial surfaces. This incision is associated with multiple phases of tectonic events and intensified climate forcing during early to mid-Holocene [23]. The sedimentation in lower reaches of river valleys is predominantly controlled by processes that act in response to tectonically triggered and climatically enhanced events [23]. The uplift involve the Bela and WH that shows abrupt and anomalous variation in elevation as noticed in the swath profiles (**Figure 1D**). The swath profiles shows maximum elevation correspond to uplifted region and low elevation correspond to valley floor. The swath analysis of each profile shows asymmetrical nature of valley shape. The results of the SL index are shown in **Figure 2A**. Integrated longitudinal river profiles with SL and Ks longitudinal profiles of all rivers are illustrated in **Figure 3**. The SL values range from 5 to 2300 which are grouped into five classes: class-1 (low activity: 5 ≤ SL ≤ 100), class-2 (intermediate activity: 101 ≤ SL ≤500), class-3 (moderate activity: 501 ≤ SL ≤ 1000), class-4 (active: 1001 ≤ SL ≤ 1500), class-5 (very active: SL ≥ 1501) (**Figure 2A**). The high and moderate classes of the SL values correspond to significant faults except for the Bela zone, may be caused by the high rock resistance prevailed in that area. The *Ks* and Θ were estimated from the log–log plot of *S* vs. *A*. The Ks values range from 5 to 125. To evaluate segmental tectonic activity; these values were also grouped into five classes: class-1 (low activity: 5 ≤ Ks ≤ 25), class-2 (intermediate activity: 26 ≤ K_S ≤ 50), class-3 (moderate activity: 51 ≤ K_S ≤ 75), class-4 (active: 76 ≤ Ks ≤ 100), and class-5 (very active: Ks >101) (**Table 1**; **Figure 2B**). It is observed that the Ks values are high close to the E-W faults.

Equation	References	Fault	(SRL km)	(RLD km)	Average RLD	Coefficient		MD (km)	AD (km)	Offset ratio (m)	Magnitude (M)	Slip rate (mm/y)
						A	B					
M = A + B * log (SRL)	[55]	F1	56	21	21	5.16	1.22				6.3-6.3-7.3	—
M = A + B * log (RA)		F2	55.6	26	5.2	3.98	1.02	3.9	1.1	0.34	5.4-6.4-7.3	3.4
M = A + B * log (MD)		F3	55.8	42.8	16.6	6.81	0.78	0.49	1.3	0.11	6.1-6.7-7.3	1.1
M = A + B*log (RLD)		F4	55.6	40.6	40.6	4.33	1.49	0.63	4.3	0.14	6.7-6.7-7.3	1.4
		F5	15.2	38.6	38.6			0.8	1.8	0.09	6.7-6.6-6.6	0.9
		F6	56.7	43.8	37.6			0.79	3.1	0.07	6.7-6.7-7.3	0.71
		F7	50	38.6	38.6			0.3	0.9	0.08	6.7-6.7-7.2	0.84
		F8	54.13	48	17.2			0.4	1	0.06	6.2-6.8-7.2	0.67
Mw = 1.36*log SRL+ 4.67	Johnston [56]	F9	21.17	19	7.2	1.36	4.67	0.8	0.9	0.14	5.6-6.2-6.7	1.4
		F10	34	33	6.6			0.3	2.2	0.31	5.6-6.5-7.0	3.1

Surface rupture length (SRL).
Sub-surface rupture length (RLD).
Standard deviation (s).
Maximum displacement (MD).
Average displacement (AD).
Moment magnitude (M).

Table 2. Regression analysis of surface rupture, subsurface rupture length, and displacement.

http://dx.doi.org/10.5772/intechopen.73653

Conventionally the hypsometric integrals reveal complex interactions between erosion and tectonics [39, 52, 53]. Hypsometric integrals are thought to be affected by basin parameters such as geometry, area and rapid lowering of basin elevations [53, 54]. The hypsometric integral of each basin has been computed based on drainage area and basin geometry. Hypsometric integrals are thought to be affected by basin parameters such as geometry, area and rapid lowering of basin elevations [53, 54]. The HI of each basin has been computed based on drainage area and basin geometry. However, we deployed conventional statistical technique for the entire basin as well as the computation is implemented to individual squire where high and low values can be obtained together. The contour map shows spatial distribution of high and low values, imply that the WH experiencing rapid changes in elevation and incision; owing to tectonic and climatic variations [23]. The higher values of HI clustered around the uplifted regions however the lower values representing low lying areas (**Figure 2C**). In the analysis of HI, it is considered whether the curve is convex in its upper portion, convex to concave, or convex in the lower portion. The HI curves of all basins are given in **Figure 4**. It is assumed that if part of the hypsometric integral is convex in the lower portion, it could be associated with uplift along a fault or associated with recent folding.

In present study 10 north flowing and 17 south flowing rivers of WH were analyzed in order to estimate river offset and tectonic control by the faults that cut across the area (**Figure 2A, B**). The estimated values of offset along F2 ranges between 1.1 and 3.9 km, along F3, 0.49–1.3 km, along F4 0.63–4.3 km, along F5 0.8–1.8 km, along F6 0.79–3.1 km, along F7 0.3–0.9 km, along F8 0.4–1 km, along F9 0.8–0.9 km, and along 10 the offset ranges between 0.3 and 2.2 km respectively (**Figure 2D**). The stream offset along the F2–10 is comparatively less westward. However, the computed values of offset ratio of about 0.34 km for F2, 0.11 km for F3, 0.14 km for F4, 0.09 km for F5, 0.07 km for F6, 0.08 km for F7, 0.06 km for F8, 0.14 km for F9 and 0.31 km for F10 respectively (**Table 2**).

8. Geomorphic evidences controlling fluvial network

We identified various geomorphic features associated with active movement along F1 such as block tilting, fault scarps, co-seismic uplift and drainage offset, are well characterized by [57]. At a place the Mesozoic sandstone ridded over Quaternary deposits, resulted ~2 m high active fault scarp (**Figure 6A–E**). The Mesozoic strata are tilted by 8° southward. We identified secondary surface deformation ~10 km along the strike of the F2 (**Figure 6A**). The co-seismic movement has developed tensional fractures along the strike of F2 (**Figure 6D–E**). The north dipping tensional fractures near F2 reflect "en echelon" pattern having step-overs with strike-slip component; probably developed during the northward movement of the hanging wall followed by surface bending (**Figure 6D** and **E**) [23].

Further Kothyari et al. [23] documented remarkable geomorphic features such as (a) E-W trending fault across gently folded Mesozoic strata, (b) steeply dipping strata with south facing active fault scarp at Deshalpar, (c) wide tensional in E-W direction, (d) highly fractured and sheared litho-units within faulted blocks, (e) subsidence of ground, and drainage offset

http://dx.doi.org/10.5772/intechopen.73653

along the structures (**Figure 6F**). The tectonic movement in this region resulted changes in surface elevation by forming approximately 9 m high fault scarp (**Figure 6G**). A significant gradient change in the valley floor causes development of 3 m high knickpoint (**Figure 6H**). The litho-units are tightly folded within the fault zone. The southern limb of the fold is steeply (~75°) dipping towards south. These steeply dipping beds are characterized by presence of slickensides parallel to the strike direction (E-W) of the F5 (**Figure 6I**). Kothyari et al. [23] believe that these features are results of middle to late Holocene tectonic reactivation of GF. Furthermore, the significant amount of changes have been observed within the hydrological network between 8 to 4 ka [23]. The north flowing Karaswali River takes 90° turn and flows in west direction, parallel to GF (F4). East–west offsetting of the two rivers is also observed south of the Gedi village (**Figure 6F**).

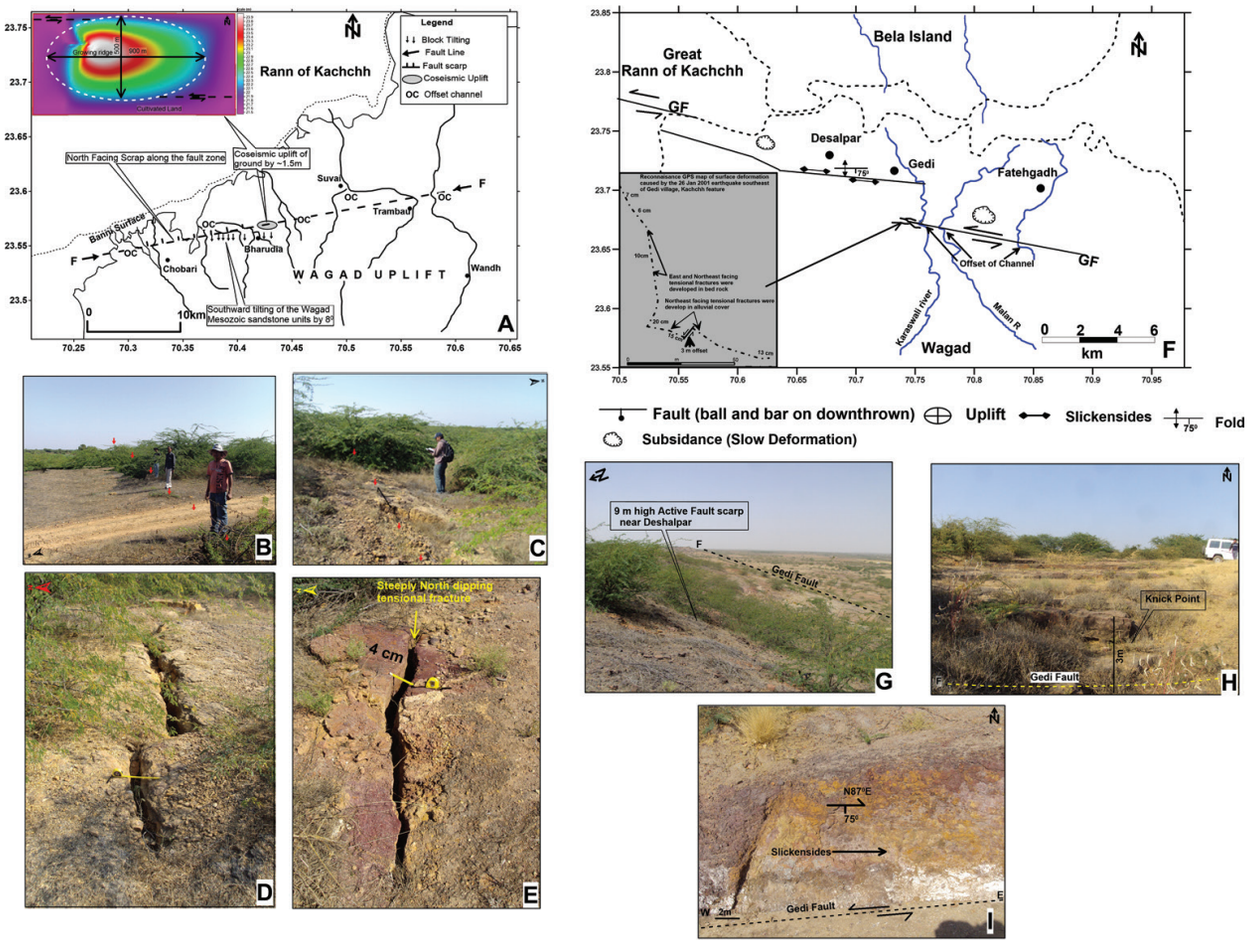

Figure 6. (A) Detailed map showing major tectonic features observed in the F2 zone (inset; DEM of growing ridge showing ground uplift (~1.5 m) near the fault zone (modified after [57]); (B and C) fault scarp; (D and E) development of E-W oriented tensional cracks within the fault zone. These tensional cracks are displaced by small scale strike slip faults. (F) Map shows locations of ground deformation observed along the trace of F4. Inset shows development of tensional fractures within the tertiary sandstone bed (modified after [23]); (G) development of ~9 m high fault scarp near Deshalpar, (H) lateral spreading of ground east of Deshalpar, and 3 m waterfall was developed along the F3, (I) well developed slickensides are visible parallel to strike of F4. *The drainage map of* **A** and **F** *are generated using georeference SOI topographic map in Global mapper 18 software and for final editing we used Surfer 14 software. The inset DEM of the area has been generated with the help of reconnaissance Real Time Kinematic (RTK) survey. The DEM has been generated in Surfer Software.*

9. Seismic tomography and fault plane solutions

The estimated velocity images and fault-plane solutions are shed new light in understanding the fluvial network and geomorphic development in the intraplate region of Western India [15]. The epicenters of the relocated earthquakes show that the majority of the events are confined along F1–F4 (**Figure 1B**) during the recorded period. It is also noticed that some of small to moderate events are located north of F4 and north of F1 (**Figure 1B**). Interestingly, epicenters of small to moderate earthquakes are associated with the offset zone of fluvial network. Theses fluvial network are plotted over seismic tomography images at 5.0 km, 10.0 km, 15.0 km, 20.0 km, 25.0 km, and 30.0 km depths to understand brittle - ductile dynamics (**Figure 7A**). Based on significant perturbations in Vp anomalies, several shallow and deep fault controlling surface fluvial network are identified. Conventionally the low velocity of Vp anomalies at shallower to deeper depths represents presence of fluid, unconsolidated rocks fault gauge, cracks and fractured basement [15, 51, 58, 59]. Based on surface fluvial offset and velocity perturbation in depth sections of tomography data, the slow velocity is interpreted as a subsurface fracture pattern or strong heterogeneities. The high velocity zones at deeper depth are associated with the surface offset of drainage network [15].

The depth slices of tomography images are critically examined to identify subsurface fault pattern (**Figure 7A**). Both combined seismological and geological results clearly show that the zone between Bharudia/NWF and IBF is controlled by eight (F1–F8) E-W oriented parallel faults. Seismic tomograms at depths 5–15 km shows NW-SE and NE-SE oriented transverse faults. The Fault F4 is a vertical fault, which is well defined by velocity perturbations sections down to the depth of 30 km depth. Faults F1, F2, F3, F5, and F6 are connected with the F4 at 25 km deeper level (**Figure 7A**, **B**). However, the fault F7 is connected with F5 at 15 km depth, whereas the F8 joints with F7 down to the depth of 10 km. **Figure 7B** represents inferred depth geometric relationship of all these faults. Geometrically all these faults are converge at depth along a single sub-vertical fault (F4), making an E-W oriented negative flower structure, where all branches of faults are interacting at different depth resulting rhomb shape graben structure (**Figure 7B**). From the experimental model of [60] it is clear that the strike–slip fault zone is generally composed of several branches that join together at depth into a single vertical plane. As a consequence, bulk displacement accommodated at depth on the basement fault is distributed towards the surface among several faults whose tectonic activity evolves through time. Some branches remain inactive during a certain period, and then they are reactivated later when their geometry becomes compatible again with the evolving strain field in the wrench zone [60]. The model shows that the local relief apparently has a clear influence on subsurface fault geometries (**Figure 7A**). In the regions of low topography or where strong river incision traverses the wrench zone, a narrow releasing bend generally develops when the fault trace is deviated towards topographic lows. In regions of higher relief, compression is often associated with shearing, and the fault zone appears much more deformed and segmented [60]. From the earthquake fault plane solution data, it is clear that all these faults are strike slip pattern in nature (**Figures 1B, 6** and **7A**). However, a few solutions show thrust motions may be due to local tectonic adjustment between segmented fault blocks.

http://dx.doi.org/10.5772/intechopen.73653

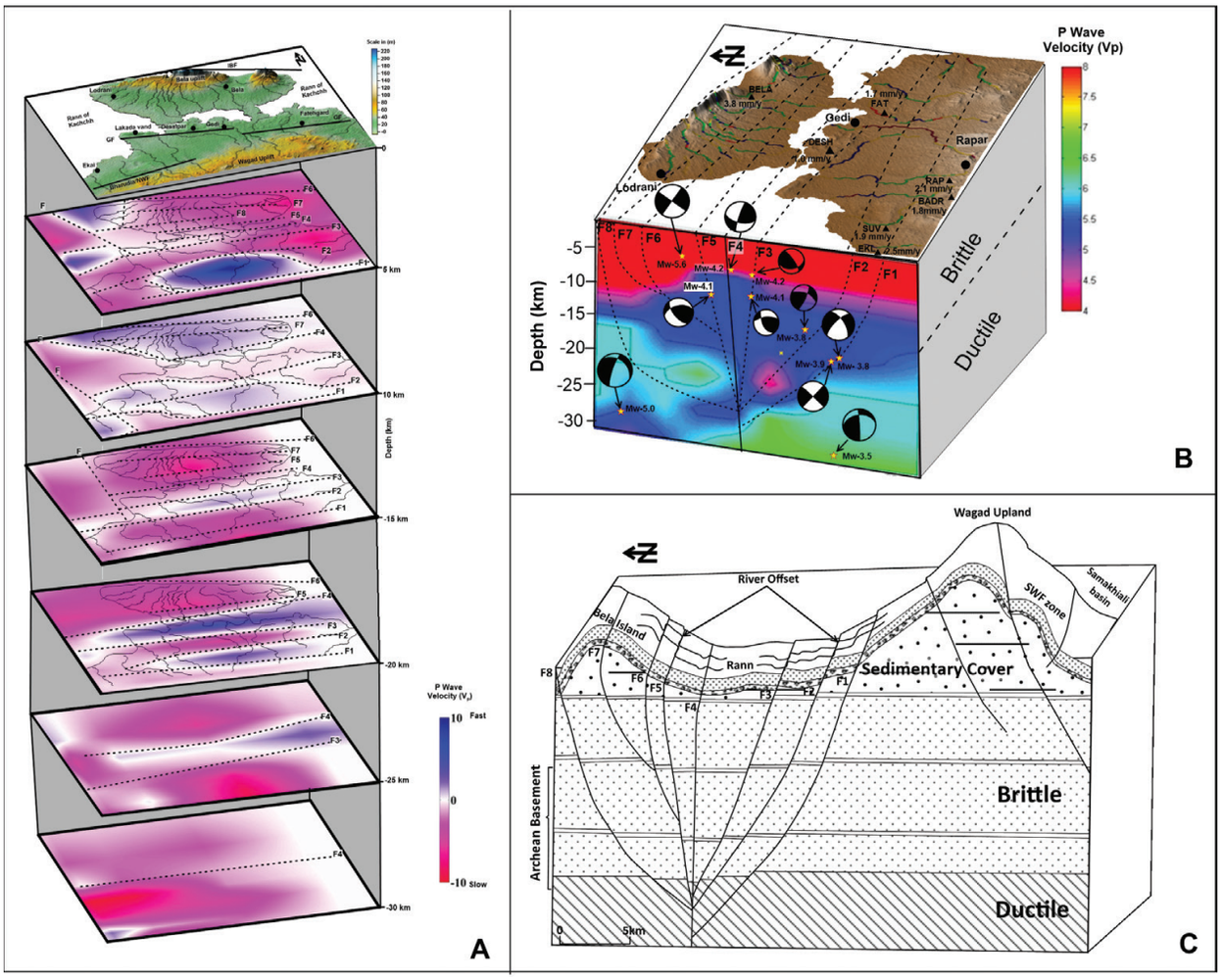

Figure 7. (A) Stack map shows horizontal depth slices of P-wave seismic structures [51] at 5, 10, 15, 20, 25, and 30 km. The topographic surface level is highlighted by digital elevation model of the area. The fault lines F1 to F10 are marked based on offset of river along the wave velocity transition phase and highlighted by black dotted lines. (B) Dimensional block model of northern Wagad areas shows development of negative flower structure at deeper level as inferred from seismic structures. The position of faults on the top surface is marked by stream offset pattern. The depth behavior of fault is shown by fault plane solutions of [12–15]. Locations on the surface are marked by black filled circles; solid fill triangles represent location of GPS stations. (C) Schematic block model of Wagad region based on geological and seismological data shows development of negative flower structure towards the northern part of the area. The streams crossing these faults show prominent offset on the surface. *The, horizontal depth slices in* **Figure 1A** *are generated using MATLAB R2010 software and depth wise stack map of horizontal slices has been generated using Surfer-14 software. The P wave velocity slice* (**B**) *has been generated in MATLAB R2010 and the final editing has been done in Surfer software. For generation of* **C** *we used CARTOSAT satellite data to generate N-S topographic profile and final map has been generated using Surfer-14 software.*

10. Combined interpretation and discussion

Globally, the rift basins are controlled by extensional tectonic forces. Changes of stress regime may cause inversion of such system from normal strike slip and reverse Coward [61], Scisciani [62] or by development of new faults between the basement rocks and overlying sedimentary succession [62, 63]. The wrench zone of a strike slip fault system shows complex arrays of structures in brittle upper crust in which fault splays are oblique to the principal fault trend

and generate a wide deformation zone [60, 64, 65]. The depth section of such faults tend to be steep at deeper level and to splay upwards, forming characteristic flower structures; have reverse (positive flower) or normal (negative flower) components [66, 67]. In such tectonic environment the shape of fault pattern is influenced by degradation and aggradation surface processes [68]. Conventionally in a negative flower zone the faults splays become listric as a result of synchronous deformation and sedimentation [69]. However, in a positive flower setting, faults tend to become steeper towards the surface as a result of aggradation in the footwall and degradation in the hanging wall [70–75].

A wide zone of fault rupture pattern is investigated in WH of Kachchh peninsula. The seismic structures, seismicity and fault plane solution investigation show that the GF (F4) is a nearly vertical fault (**Figure 7B**, **C**) having dominant strike-slip deformation [15, 18, 51]. Using double difference tomography, we identified several shallower and deeper faults (F1–10); these faults are well connected with sub-vertical south dipping GF (F4) at different level (**Figure 7B** and **C**). Geometrical relationship inferred from seismic structures show all these faults are converge at certain depth along GF and making E-W oriented negative flower structure. All fault branches are interacting at different depth level and generating rhomb shape graben structure, which is well imaged in the seismic structures (**Figure 7B** and **C**). Depth section of tomography suggested that the faults F1, F2, F3, F5 and F8 are deeper faults. However, the F6 and F7 are imaged at shallower depth. It is also clear from the seismic structures that the fault F1 is a north dipping fault plane and connected with the F4 at 27 km depth level. The north dipping faults F2 and F3 and the south dipping faults F5 and F8 are connected with F4 at 25 km depth level. On the other hand the fault F6 is a southward dipping splay of F5 and connected with F5 at 15 km depth. The F7 is a small south dipping subsidiary branch of F6. The fault is connected with F6 at 12 km depth.

Conventionally, an extensional overstep zone of a strike–slip fault several branches that join together at depth into a single vertical plane [18]. As a consequence, bulk displacement accommodated at depth on the basement fault is distributed towards the surface among several faults whose tectonic activity evolves through time [60]. Some branches remain inactive during a certain period, and then they are reactivated later when their geometry becomes compatible again with the evolving strain field in the wrench zone [60]. A few researchers argued that KRB regions show dominantly strike-slip with the slightly reverse faulting natures [13, 51, 76]. However, a few solution shows reverse type of motion could be associated with the local tectonic adjustment between segmented fault blocks.

The archeological records from the WH experience several damaging earthquakes of magnitude 6.0–7.8; that have occurred between 2900 BC and 1300 BC (**Table 3**). The archeological evidences observed from 40 km west of study area (e.g. Dholavira) suggested that the ancient town was damaged by several major earthquakes between 2900BC and 1300BC [63, 77–79]. Presence of geomorphic and paleoseismic features within the WH, studied by previous workers are correlated with these historical earthquakes [23, 25, 63]. Further, based on trench investigation and optical chronology identified three earthquake events during last 7000 years [63]. The displaced fluvial sediment and optical chronology in the area suggested that the SWF reactivated during Middle to Late Holocene period i.e., between 3 ka and 1 ka [25]. Similarly other geomorphic studies suggest that the F4 reactivated during Middle Holocene around 4 ka [23].

In-SAR measurements show current deformation rate as ~16 mm/y in the western part and 7–16 mm/y in the southern part of the GF zone [14, 23, 80]. Based on trench investigation [63] estimated uplift rate of 0.5 ± 0.05 mm/y, horizontal shortening rate of 1.1 ± 0.12 mm/y along SWF. However based of fluvial offset [25] estimated slip rate 2.2 mm/y along the SWF zone which is compatible with the slip rate 1.19 ± 0.13 mm/y observed by [63]. Based on strath terraces [23] estimated the uplift rates 0.3 to 1.1 mm/y along F4, during the last 9 ka. Further, based on fluvial offset, we estimated slip rates for faults (F2–F10) using the imperial relationship given by [45]. The estimated slip rate along F2 of about 3.4 mm/y, along F3 of about 1.1 mm/y, along F4 of about 1.4 mm/y. along F5 of about 0.9 mm/y, along F6 of about 0.71 mm/y, along F7 of about 0.84 mm/y, along F8 of about 0.67 mm/y, along F9 of about 1.4 mm/y, and along F10 of about 3.1 mm/y (**Table 2**). The observed slip rate of F2–F10 are well corroborated with the uplift rate 0.3 to1.1 mm/y during the last 9 ka as estimated from the OSL dates. The slip rates obtained from drainage analysis are well correlated with the published results of GPS from the WH (ISR technical report by [81]. Four sites located in the southern part of study area shows variations in localized deformation (**Figure 7B**). The site Ekal shows deformation rate 2.5 ± 0.12 mm/y, Suvai is deforming at the rate of 1.9 ± 0.03 mm/yr., Badargadh is deformation at the rate of 1.8 ± 0.13 mm/y, and the site located near Rapar shows deformation rate of 2.1 ± 0.11 mm/y [81]. To sites Deshalpar and Fatehgadh shows deformation rates of 1.0 ± 0.04 mm/y and 1.7 ± 0.04 mm/y (**Figure 7B**). However, a site located in the northern part of study area shows crustal deformation rate 3.8 ± 0.14 mm/y [81]. The estimated slip rates and GPS driven deformation rates together suggests that the landform development in the area is controlled by localized crustal deformation.

The future earthquake along active faults can be evaluated from estimates of fault rupture parameter in turn, released to earthquake magnitude [55]. Active fault studies require an assessment of seismic hazard analysis for the future potential earthquakes [55]. More specifically to estimate the size of earthquake that might be generated by a particular fault may be correlated with rupture parameter such as length, strike and displacement [55, 82, 83]. Moreover, the timing of the past earthquake and size of magnitude can be estimated with the help of geomorphic and paleoseismic records [84, 85]. We used regression analysis proposed by Wells and Coppersmith [55] and by Johnston [56] and Johnston and Kanter [86] for intraplate region to estimate moment magnitude. The detail regression analysis is expressed

S. No	Year	Remarks	References
1	2900BC	Damage in Dholavira, dislocation of walls, subsidence of floors and crushed bricks	[77]
2	2700BC	Damage in Dholavira, 4 m wide fissured wall, collapse of southern features and multiple cracks running E-W	[78]
3	2100BC	Damage in Dholavira; tremendous damage to the gates of castle, tilting and arching of thick inner walls and collapse of outer walls at north gate	[79]
4	2000BC		
6	1900BC	Abandonment of settlements	[63]
7	1300BC		

Table 3. List of historic earthquakes occurred in Kachchh region of western India.

in **Table 2**. The regression analysis proposed by Wells and Coppersmith [55] and Johnston [56] shows strong correlation between surface rupture length and magnitude of earthquakes. However the regression analysis shows that probability of occurrence of earthquake magnitude range between 6.3 and 7.3) along F1, magnitude (M 5.4–M 7.3) along F2, magnitude (M 6.1–M 7.3) along F3, magnitude (M 6.7–M 7.3) along F4, magnitude (M 6.0–M 6.6) along F5, magnitude (M 6.7–M 7.3) along F6, magnitude (M 6.7–M 7.2) along F7, magnitude (M 6.2–M 7.2) along F8, magnitude (M 5.6- M 6.7) along F9, magnitude (M 5.6–M 7.0) along F10 respectively (**Table 2**). From the regression analysis it is clear that the faults (F1–F10) passes through the WH are capable for generating earthquake magnitude M 5.4 and M 7.3. Occurrence of February 2006M-5.6 along F9 validates our results and significant level.

Geomorphic indices are widely used to obtain index of active tectonics [25, 48–50]. Here we synthesized conventional geomorphic indices of active tectonics to calculate relative index of active tectonic (RIAT) distribution along the all fault segments (F1–F10). The RIAT classes show that the deformation is higher along the offset zone of fault segment (**Figure 5B**). Conventionally the SL and KS values show abnormal increase of gradient within normal and reverse faults. Minor changes of SL and KS observed within the zone of strike slip fault. At few places the SL and KS values do not shows any variation, which is compared with the strike slip motion of fault. The strike slip motion is well corroborated with the results of seismic tomography and fault plane solution (**Figure 7B**). The existing studies suggest that the terrain close to the GF (F4) experienced occurrence of moderate earthquakes during recent time [23, 27]. The strike slip motion observed from focal mechanism is well correlated with drainage offset along E-W oriented faults within the north and south flowing river system.

Further the observations gathered from the SL, KS and RIAT distribution are corroborated with the geomorphological studies carried out by [23]. The geomorphic expressions such as active fault scarp, shifting and offset of channels indicates that the area is controlled by E-W oriented strike slip faults. Further, steepening of river gradient as observed from tectonic proxy (SL and KS) and uplift of ground further support that the area is tectonically active. Previous studies by [23] suggests that the uplifts in GF zone were associated with interlinking of strike slip fault segments. Further major two phase of tectonic uplift have been identified by [23] based on uplifted fluvial strath terraces. The study shows that the first phase of enhanced uplift took place round 8.0 ± 0.9 ka; however, the second phase of uplift is began after 4 ka and continued till today [23]. In present study, several E-W oriented knickpoints were identified across north and south flowing drainage basins of WH. At several locations these knick points have migrated primarily due to river response to sudden base level fall and secondly incision owing to vertical tectonic forces. As sudden base-level fall can be triggered by tectonic upheaval, climatic change, river capture, or channel incision [87–89]. The incision by river and the formation of knickpoints are well correlated with tectonic upheaval along F1–F8 (**Figure 2A**).

11. Conclusions

The study of the topographic configuration morphometric analysis and the subsurface imaging of the fluvial network from WH permitted us to develop a model for the long-term

http://dx.doi.org/10.5772/intechopen.73653

evolution of the drainage basin which is influence by deep tectonic processes. Based on present observations the following conclusions have been drawn.

1. Based on analysis of fluvial offset and subsurface velocity images major 10 traces of active fault (F1–F10) controlling hydraulic network have been identified.
2. The surface geomorphology, velocity imaging and fault plane solution data together suggest that the subsurface structure of WH is controlled by strike slip faulting.
3. The fault geometry inferred from seismic images show presence of negative flower structure at a deeper level.
4. The depth wise images show that the GF (F4) is steeply dipping towards south. The fault F1, F2 and F3 are dipping towards north, whereas, the fault F5–F8 are dipping towards south. All these faults are connected with GF (F4) at different depth level, which is well imaged in the seismic structures.

Acknowledgements

The authors are thankful to Ministry of Earth Science, Government of India (MoES/P.O.(Seismo)/1(270)/AFM/2015) for financial support under the active fault mapping program. We are thankful to Dr. M. Ravikumar, Director General and Dr. Sumer Chopra, Director, Institute of Seismological Research, Gandhinagar for fruitful discussion.

Conflict of interest

There is no conflict of interest between all co-authors.

Author's contribution

All the authors have made equal contribution in this manuscript.

Author details

Girish Ch Kothyari*, Ajay P. Singh, Sneha Mishra, Raj Sunil Kandregula, Indu Chaudhary and Gaurav Chauhan

*Address all correspondence to: kothyarigirish_k@rediffmail.com

Institute of Seismological Research, Gandhinagar, Gujarat, India

References

[1] Sembroni A, Molin P, Pazzaglia FJ, Faccenna C, Abebe B. Evolution of continental-scale drainage in response to mantle dynamics and surface processes: An example from the Ethiopian highlands. Geomorphology. 2016;**261**:12-29

[2] Pazzaglia FJ, Gardner TW, Merritts DJ. Bedrock fluvial incision and longitudinal profile development over geologic time scales determined by fluvial terraces. In: Wohl E, Tinkler K, editors. River over Rock: Fluvial Processes in Bedrock Channels American Geophysical Union Geophysical Monograph 107. Washington, DC: American Geophysical Union; 1998. pp. 207-235

[3] Scotti VN, Molin P, Faccenna C, Soligo M, Casas-Sainz A. The influence of surface and tectonic processes on landscape evolution of the Iberian chain (Spain): Quantitative geomorphological analysis and geochronology. Geomorphology. 2014. DOI: 10.1016/j.geomorph.2013.09.017

[4] Tomkin JH, Brandon MT, Pazzaglia FJ, Barbour JR, Willett SD. Quantitative testing of bedrock incision models, Clearwater River, NW Washington state. Journal of Geophysical Research. 2003;**108**(B6). DOI: 10.1029/2001JB000862

[5] Wegmann KW, Zurek BD, Regalla CA, Bilardello D, Wollenberg JL, Kopczynski SE, Ziemann JM, Haight SL, Apgar JD, Zhao C, Pazzaglia FJ. Position of the Snake River watershed divide as an indicator of geodynamic processes in the greater Yellowstone region, western North America. Geosphere. 2007;**3**(4):272-281

[6] Wegmann KW, Pazzaglia FJ. Holocene strath terraces, climate change, and active tectonics: The Clearwater River basin, Olympic peninsula, Washington state. Geological Society of America Bulletin. 2002;**114**:731-744

[7] Wells SG, Bullard TF, Menges CM, Drake PG, Karas PA, Kelson KI, Ritter JB, Wesling JR. Regional variations in tectonic geomorphology along a segmented convergent plate boundary, Pacific coast of Costa Rica. Geomorphology. 1988;**1**:239-265

[8] Wobus C, Whipple KX, Kirby E, Snyder N, Johnson J, Spyropolou K, Crosby B, Sheehan D. Tectonics from topography: Procedures, promise, and pitfalls. In: Willett SD et al., editors. Tectonics, Climate, and Landscape Evolution. Geol. Soc. Am. Vol. 398. 2013. pp. 55-74

[9] Molin P, Fubelli G, Nocentini M, Sperini S, Ignat P, Grecu F, Dramis F. Interaction of mantle dynamics, crustal tectonics and surface processes in the topography of the Romanian Carpathians: A geomorphological approach. Global and Planetary Change. 2012. DOI: 10.1016/j.gloplacha.2011.05.005

[10] Biswas SK. A review of structure and tectonics of Kutch basin, western India with special reference to earthquakes. Current Science. 2005;**88**(10):1592-1600

[11] Biswas SK, Deshpande SV. Geologic and tectonic maps of Kachchh. Bull ONGC. 1973;**7**: 115-116

[12] Mandal P, Chadha RK, Raju IP, Kumar N, Satyamurty C, Narsaiah R. Are the 7th march 2006 Mw 5.6 event and the 3rd February 2006 Mw 4-5.8 event triggered by the five years continued occurrence of aftershocks of the 2001 Mw 7.7 Bhuj event. Current Science. 2007;**92**:1114-1124

[13] Rao CN, Rao PC, Rastogi BK. Evidence for right–lateral strike-slip environment in the Kutch basin of northwestern India from moment tensor inversion studies. Journal of Asian Earth Sciences. 2014;**64**:158-167

[14] Rastogi BK, Mandal P, Biswas SK. Seismogenesis of earthquakes occurring in ancient rift basin of Kachchh, western India. In: Talwani P, editor. Intraplate Earthquakes. Cambridge; 2014. pp. 126-161

[15] Singh AP, Dorbath C, Kumar MR, Kumar S, Chaudhary I, Kayal JR. Fault geometry of the M 7.7 western India Intraplate earthquake: Constrained from double-difference tomography and fault-plane solutions. Bulletin of the Seismological Society of America. 2016a. DOI: 10.1785/0120150280

[16] Biswas SK. Regional tectonic framework, structure and evolution of the western margin basins of India. Tectonophysics. 1987;**135**:307-327

[17] Biswas SK. Tectonic framework, structure and tectonic evolution of Kutch Basin, western India. Special publication of the Geological Society of India. 2016;(6):129-150

[18] Kothyari GC, Dumka RK, Singh AP, Chauhan G, Thakkar MG, Biswas SK. Tectonic evolution and stress pattern of south Wagad fault at the Kachchh Rift Basin in western India. Geological Magazine. 2016c;**154**(4):875-887

[19] Mandal P, Rastogi BK, Satyanarayana HVS, Kousalya M, Vijayraghavan R, Satyamurty C, Raju IP, Sarma ANS, Kumar N. Characterization of the causative fault system for the 2001 Bhuj earthquake of Mw 7.7. Tectonophysics. 2004;**378**:105-121

[20] Kayal JR, De R, Ram S, Sriram BV, Gaonkar SG. Aftershocks of 26th January Bhuj earthquake in western India and its seismotectonic implication. Journal Geological Society of India. 2002;**59**:395-418

[21] Singh AP, Mishra OP, Rastogi BK, Kumar D. 3-D seismic structure of the Kachchh, Gujarat and its implications for the earthquake hazard mitigation. Natural Hazards. 2011;**57**:83-105

[22] Bodin P, Horton S. Source parameters and tectonic implications of aftershocks of the M 7.6 Bhuj earthquake of 26 January 2001. Bulletin of the Seismological Society of America. 2004;**94**:818-827

[23] Kothyari GC, Rastogi BK, Morthekai P, Dumka RK. Landform development in a zone of active Gedi fault, eastern Kachchh Rift Basin, western India. Tectonophysics. 2016b; **670**:115-126

[24] Bhattacharya F, Rastogi BK, Kothyari GC. Morphometric evidences of seismicity around Wagad and Gedi faults, eastern Kachchh, Gujarat. Journal of the Geological Society of India. 2013;**81**:113-121

[25] Kothyari GC, Rastogi BK, Morthekai P, Dumka RK, Kandregula RS. Active segmentation assessment of the tectonically active south Wagad fault in Kachchh, western peninsular India. Geomorphology. 2016a;**253**:491-507

[26] Biswas SK. Landscape of Kutch—A morphotectonic analysis. Indian Journal of Earth Sciences. 1974;**1**(2):177-190

[27] Mandal P, Satyamurty C, Raju IP. Iterative de-convolution of the local waveforms: Characterization of the seismic sources in Kachchh, India. Tectonophysics. 2009;**478**: 143-157

[28] Molin P, Pazzaglia FJ, Dramis F. Geomorphic expression of active tectonics in a rapidly deforming forearc, Sila massif, Calabria, southern Italy. American Journal of Science. 2004;**304**:559-589

[29] Duncan C, Masek J, Fielding E. How steep are the Himalaya? Characteristics and implications of along-strike topographic variations. Geology. 2003;**31**:75-78

[30] Ponza A, Pazzaglia FJ, Picotti V. Thrust-fold activity at the mountain front of the northern Apennines (Italy) from quantitative landscape analysis. Geomorphology. 2010;**123**: 211-231

[31] Andreani L, Gloaguen R. Geomorphic analysis of transient landscapes in the sierra Madre de Chiapas and Maya Mountains (northern central America): Implications for the north American–Caribbean–Cocos plate boundary. Earth Surface Dynamics. 2016;**4**:71-102

[32] Keller EA, Pinter N. Active Tectonics. Earthquake, Uplift, and Landscape. New Jersey: Prentice Hall; 2002. p. 362

[33] Troiani F, Troiani M, Della S. The use of the stream length-gradient index in morphotectonic analysis of small catchments: A case study from Central Italy. Geomorphology. 2008;(1):159-168

[34] Hack J. Drainage adjustment in the Appalachians. In: Morisawa M, editor. Fluvial Geomorphology. London: George llen and Unwin; 1973. pp. 51-69

[35] Merrits D, Vincent KR. Geomorphic response of coastal streams to low, intermediate, and high rates of uplift, Mendocino triple junction region, northern California. Geological Society of America Bulletin. 1989;**101**:1373-1388

[36] Flint JJ. Stream gradient as a function of order, magnitude, and discharge. Water Resources Research. 1974;**10**:969-973

[37] Goldrick G, Bishop P. Regional analysis of bedrock streamlong profiles: Evaluation of Hack's SL form, and formulation and assessment of an alternative (the DS form). Earth Surface Processes and Landforms. 2007;**32**(5):649-671

[38] Whipple KX, Di-Biase RA, Crosby BT. Bedrock Rivers. Treatise on Geomorphology. 2013;**9**:550-570

[39] Strahler AN. Hypsometric (area-altitude) analysis of erosional topography. Geological Society of America Bulletin. 1952;**63**:1117-1142

[40] Menéndez I, Silva PG, Martín-Betancor M, Pérez-Torrado FJ, Guillou H, Scaillet S. Fluvial dissection, isostatic uplift, and geomorphological evolution of volcanic islands (gran Canaria, Canary Islands, Spain). Geomorphology. 2008;**102**:189-203

[41] Bull WB, McFadden LD. Tectonic geomorphology north and south of the Garlock fault, California. In: Doehering DO, editor. Geomorphology in Arid Regions. Proceedings at the Eighth Annual Geomorphology Symposium. Binghamton, NY: State University of New York; 1977. pp. 115-138

[42] Pérez-Peña JV, Azor A, Azañón JM, Keller EA. Active tectonics in the sierra Nevada (Betic cordillera, SE Spain): Insights from geomorphic indeces and drainage pattern analysis. Geomorphology. 2010;**119**:74-87

[43] Ramírez-Herrera MT. Geomorphic assessment of active tectonics in the Acambay Graben, Mexican volcanic belt. Earth Surface Processes and Landforms. 1998;**23**:317-332

[44] Malik JN, Nakata T. Active faults and related late quaternary deformation along the north-western Himalayan frontal zone, India. Annales de Geophysique. 2003;**46**(5):917-936

[45] Matsuda T. Active Fault Assessment for Irozaki Fault System, Izu Peninsula. Report on the Earthquake of the Izu Peninsula. 1975;**38**:409p

[46] Bull WB. Tectonic Geomorphology of Mountains: A New Approach to Paleoseismology. Malden: Blackwell; 1977

[47] Matsuda T. Strike-Slip Faulting along the Atera Fault, Japan. Univ. Tokyo Earthq. Res. Inst. Bull. vol. 44; 1966. pp. 103-111

[48] Azor A, Keller EA, Yeats RS. Geomorphic indicators of active fold growth: South Mountain, oak ridge anticline, Ventura basin, southern California. Geological Society of America Bulletin. 2002;**114**:745-753

[49] Rockwell TK, Keller EA, Johnson DL. Tectonic geomorphology of alluvial fans and mountain fronts near Ventura, California. In: Morisawa M, editor. Tectonic Geomorphology. In: Proceedings of the 15th Annual Geomorphology Symposium. Boston: Allen and Unwin Publishers; 1985. pp. 183-207

[50] Silva PG, Goy JL, Zazo C, Bardají T. Fault generated mountain fronts in Southeast Spain: Geomorphologic assessment of tectonic and seismic activity. Geomorphology. 2003;**50**:203-225

[51] Singh AP, Zhao L, Kumar S, Mishra S. Inversions for earthquake focal mechanisms and regional stress in the Kachchh rift basin, western India: Tectonic implications. Journal of Asian Earth Sciences. 2016b;**117**:269-283

[52] Hurtrez JE, Lucazeau F, Lave J, Avouac JP. Investigation of the relationships between basin morphology, tectonic uplift, anddenudation from the study of an active fold belt in the Siwalik Hills, Central Nepal. Journal of Geophysical Research: Solid Earth. 1999;**104**:12779-12796

[53] Pérez-Peña JV, Azañón JM, Booth-Rea G, Azor A, Delgado J. Differentiating geology and tectonics using a spatial autocorrelation technique for the hypsometric integral. Journal of Geophysical Research. 2009;**114**. DOI: 10.1029/2008JF001092

[54] Chen YC, Sung Q, Cheng KY. Along-strike variations of morphotectonic features in the western foothills of Taiwan: Tectonic implications based on stream-gradient and hypsometric analysis. Geomorphology. 2003;**56**:109-137

[55] Wells DL, Coppersmith KJ. New empirical relationships among magnitude, rupture length, rupture width, rupture area, and surface displacement. Bulletin of the Seismological Society of America. 1994;**84**:974-1002

[56] Johnston AC. Seismotectonic Interpretations and Conclusions from the Stable Continental Regions. The Earthquakes of Stable Continental Regions: Assessment of Large Earthquake Potential. Palo Alto: Electric Power & Research Institute; 1994. Report TR 10261 Ch.3

[57] Kothyari GC, Rastogi BK, Dumka RK, Chauhan M. Secondary surface deformation along the Bharudia/north Wagad fault zone in Kachchh Rift Basin, western India. Comunicações Geológicas. 2015;**102**(1):15-27

[58] Mishra OP, Singh AP, Rastogi BK. An insight crack density, saturation rate, and porosity model of the 2001 Bhuj earthquake in the stable continental region of western India. Journal of Asian Earth Sciences. 2014;**83**:48-59

[59] Singh AP, Mishra OP. Seismological evidence for monsoon induced micro to moderate earthquake sequence beneath the 2011 Talala, Saurashtra earthquake, Gujarat, India. Tectonophysics. 2015;**611**:38-48

[60] Graveleau F, Strak V, Dominguez S, Malavieille J, Manighetti I, Petit C. Experimental modelling of tectonics–erosion–sedimentation interactions in compressional, extensional, and strike–slip settings. Geomorphology. 2015. DOI: 10.1016/j.geomorph.2015.02.011

[61] Coward MP. Continental collision. In: Hancock PL, editor. Inversion Tectonics. New York: Pergamon Press; 1994. pp. 289-304

[62] Scisciani V. Styles of positive inversion tectonics in the central Apennines and in the Adriatic foreland: Implications for the evolution of the Apennine chain (Italy). Journal of Structural Geology. 2009;**31**:1276-1294

[63] Malik JN, Gadhavi MS, Kothyari GC, Sathuluri S. Paleo-earthquake signatures from the south Wagad fault (SWF), Wagad Island, Kachchh, Gujarat, western India: A potential seismic hazard Journal of Structural Geology. 2017;**95**:142-159

[64] Naylor MA, Mandl G, Sijpesteijn CHK. Fault geometries in basement-induced wrench faulting under different initial stress states. Journal of Structural Geology. 1986;**8**:737-752

[65] Tchalenko JS. Similarities between shear zones of different magnitudes. Geological Society of America Bulletin. 1970;**81**:1625-1640

[66] Harding TP. Seismic characteristics and identification of negative flower structures, positive flower structures, and positive structural inversion. AAPG Bulletin. 1985;**69**(4): 582-600

[67] Sylvester AG. Strike-slip faults. Geological Society of America Bulletin. 1988;**100**:1666-1703

[68] Guerroue EL, Cobbold PR. Influence of erosion and sedimentation on strike slip fault system: Insights from analogue model. Journal of Structural Geology. 2006;**28**:421-430

[69] Vendeville B, Cobbold PR. How normal faulting and sedimentation interact to produce listric fault profiles and stratigraphic wedges. Journal of Structural Geology. 1988;**10**:649-659

[70] Barrier L, Nalpas T, Gapais D, Proust JN, Casas AM, Bourquin S. Influence of syntectonic sedimentation on thrust geometry. Field examples from the Iberian chain (Spain) and analogue modelling. Sedimentary Geology. 2002;**146**(1-2):91-104

[71] Cobbold PR, Davy P, Gapais D, Rossello EA, Sadybakasov E, Thomas JC, Tondji Biyo JJ, De Urreiztieta M. Sedimentary basins and crustal thickening. Sedimentary Geology. 1993;**86**:77-89

[72] Davy P, Cobbold PR. Experiments on shortening of a 4-layer model of the continental lithosphere. Tectonophysics. 1991;**188**(1-2):1-25

[73] Persson KS, Sokoutis D. Analogue models of orogenic wedges controlled by erosion. Tectonophysics. 2002;**356**:323-336

[74] Storti F, McClay K. Influence of syntectonic sedimentation on thrust wedges in analogue models. Geology. 1995;**23**:999-1002

[75] Tondji Biyo JJ. Chevauchements et basins compressifs influence de l'erosion et de la sedimentation. Modelisation analogique et exemples naturels. Memoires de Geosciences-Rennes. 1995;**59**:1-411

[76] Mandal M, Horton S. Relocation of aftershocks, focal mechanisms and stress inversion: Implications toward the seismotectonics of the causative fault zone of Mw 7.6 2001 Bhuj earthquake (India), Tectonophysics. 2007;**429**:61-78

[77] Bisht RS. Major earthquake occurrences in archaeological strata of Harappan settlement at Dholavira (Kachchh, Gujarat) (abstract). In: International Symposium on the 2001 Bhuj Earthquake and Advances in Earthquake Science (AES-2011), Gandhinagar. 2011. pp. 22-24

[78] Gaur AS, Vora KH, Sundaresh RMM, Jayakumar S. Was the Rann of Kachhh naviagable during the Harappan times (mid-Holocene)? An archaeological perspective. Current Science. 2013;**105**(11):1485-1491

[79] Kovach RL, Grijalva K, Nur A. **earthquakes and civilizations of the Indus Valley: A challenge for archaeoseismology. In: Sintubin M, Stewart IS, Niemi TM, Altunel E, editors. Ancient Earthquakes: Geological Society of America Special Paper. 471. 2010. pp. 119-127

[80] Rastogi BK, Choudhury P, Dumka RK, Sreejith KM, Majumdar TJ. Stress pulse migration by viscoelastic process for long-distance delayed triggering of shocks in Gujarat, India, after the 2001 Mw 7.7 Bhuj earthquake. American Geophysical Union. 2012;**196**:63-73

[81] Dumka RK, Rastogi BK, Chodhury P, Kumar P, Prajapati S. Crustal Deformation Studies by GPS Measurements. ISR Annual Report; 2015. pp 64-66

[82] Chinnery MA. Earthquake magnitude and source parameters. Bulletin of the Seismological Society of America. 2003;**59**:1969-1982

[83] Tocher D. The Alaska earthquake of July 10, 1958-movement on the fairweather fault and field investigation of southern epicentral region. Bulletin of the Seismological Society of America. 1960;**50**:267-292

[84] Coppersmith KJ. Seismic source characterization for engineering seismic hazard analysis. In: Proc. 4th International Conference on Seismic Zonation. Vol. I. Oakland, California: Earthquake Engineering Research Institute; 1991. pp. 3-60

[85] Schwartz DP, Coppersmith KJ. Seismic Hazards New Trends in Analysis Using Geologic Data, in Active Tectonics. Washington, D.C.: National Academy Press; 2009. pp. 215-230

[86] Johnston AC, Kanter LR. Earthquakes in stable continental crust. Scientific American. 1990;**262**:68-75

[87] Seidl MA, Dietrich WE, Kirchner JW. Longitudinal profile development into bedrock: An analysis of Hawaiian channels. Journal of Geology. 1994;**102**:457-474

[88] Stock JD, Montgomery DR. Geologic constraints on bedrock river incision using the stream power law. Journal of Geophysical Research. 1999;**104**(B3):4983-4993

[89] Weissel JK, Seidl MA. Inland propagation of erosional escarpments and river profile evolution across the southeast Australian passive continental margin. In: Tinkler KJ, Wohl EE, editors. Rivers over Rock: Fluvial Processes in Bedrock Channels. Geophysical Monograph. Vol. 107. 1998. pp. 189-206